

Synthesis of Self-Assembled Porous Naphtalene Dianhydride-TiO₂ Composites for Photocatalytic Hydrogen Production

Yifan Chen, Derui Kong, Lianfen Chen, Peter VanNatta, Hang Li, Jiaao Cheng, Chengzhi Ma, Pinghuai Liu, Yujie Song, Shanshuai Chen,* Cheng-Xia Chen,* Thamraa AlShahrani, and Shengqian Ma*

Conversion of solar energy to clean energy via naphthalenetetracarboxylic dianhydride (ND)-based organic semiconductors represents a topic of research. Nonetheless, efforts in this area are challenging due to the rapid recombination of photogenerated electron-hole (e-h) pairs arising from over-accumulation. Herein, various *n*-type hybrid photocatalysts, ND-TiO₂ (*x*:*y*) (*x* and *y* represent the ratios of ND and TiO₂, respectively), featuring excellent visible-light responsiveness, fast separation and migration ability of charge carriers, and permanent porosity, are constructed via a sol-gel self-assembly approach. The rational assembly of ND with TiO₂ not only effectively inhibits the problematic overgrowth of ND but also enables the composites with excellent visible-light responsiveness, and facilitates the separation and migration of charge carriers, thus resulting in greatly improved photocatalytic H₂ evolution performance. The optimized composite ND-TiO₂(1:10) with 0.38 wt% Pt nanoparticle loading presents a maximum hydrogen-evolution rate of 3.23 mmol·g⁻¹·h⁻¹, with extraordinary TON (2446) and TOF (163.1 h⁻¹), which are much higher than ND (0.031 mmol·g⁻¹·h⁻¹) and TiO₂-Colloid (0.027 mmol·g⁻¹·h⁻¹) counterparts. In addition, the underlying photocatalytic mechanism is well established through comprehensive experiments and computational studies.

1. Introduction

The conversion of solar energy to sustainable and renewable energy as an alternative to conventional fossil fuels represents one of the most promising methodologies to address the increasingly serious energy crisis and environmental pollution.^[1] In this respect, the visible-light-driven photocatalytic H₂ production from water splitting has drawn extensive attention due to its cost-efficiency and environmental friendliness.^[2] Up to now, enormous effort has been dedicated to developing various catalysts for enhancing the photocatalytic H₂ evolution performance, such as MOF/COF composites, conjugated polymers, and porous carbon nitride materials.^[3] However, achieving strong visible-light responsiveness, rapid separation, and migration of photogenerated charge carriers, as well as excellent sustainable

Y. Chen, D. Kong, H. Li, J. Cheng, C. Ma, P. Liu, Y. Song, S. Chen
School of Chemistry and Chemical Engineering
Hainan University
Haikou 570228, China
E-mail: chenss92@hainanu.edu.cn

C.-X. Chen
MOE Laboratory of Bioinorganic and Synthetic Chemistry
GBRCE for Functional Molecular Engineering
Lehn Institute of Functional Materials
IGCME
School of Chemistry
Sun Yat-Sen University
Guangzhou 510006, China
E-mail: chenchx29@mail.sysu.edu.cn

S. Chen
Sanya Nanfan Research Institute of Hainan University
Hainan University
Sanya 572025, China

P. VanNatta, S. Ma
Department of Chemistry
University of North Texas CHEM 305D
1508 W Mulberry St, Denton, Texas 76201, USA
E-mail: shengqian.ma@unt.edu

L. Chen
Guangdong Provincial Key Laboratory of Eco-environmental Studies and Low-carbon Agriculture in Peri-urban Areas
School of Environmental and Chemical Engineering
Zhaoqing University
Zhaoqing 526061, China

T. AlShahrani
Department of Physics
College of Science
Princess Nourah bint Abdulrahman University
11564
Riyadh, Saudi Arabia

 The ORCID identification number(s) for the author(s) of this article can be found under <https://doi.org/10.1002/smll.202501964>

DOI: 10.1002/smll.202501964

recyclability, remains highly challenging.

Recently, *n*-type organic semiconductors have garnered enormous attention in the fields of electronic and photonic devices,^[4] organic solar cell,^[5] gas separation membrane materials,^[6] and lithium-ion batteries,^[7] owing to their exceptional ability to transport electrons, strong electron affinity of lowest unoccupied molecular orbital (LUMO), and potential application as large area flexible circuits. Particularly, self-assembled supramolecular semiconductors through π - π stacking between organic semiconductors, such as tetracyanoquinodimethane (TCNQ),^[8] 1,4,5,8-naphthalenetetracarboxylic dianhydride (ND),^[9] perylene-3,4,9,10-tetracarboxylic dianhydride (PTCDA),^[10] and their tetracarboxylic diimide derivatives, exhibit outstanding charge carrier migration capability, tunable band gap, ordered structure, as well as extraordinary stability.^[11] Generally, the self-assembled supramolecular semiconductors with π -conjugated plane structures are H- and J-type aggregates depending on the side-chain steric hindrance and hydrophilicity/hydrophobicity of the organic monomers. The H-type aggregates are constructed from the organic monomer with short and hydrophilic side-chains through face-to-face arrangement, while the J-type aggregates are synthesized from the organic monomers with long and hydrophobic side-chains via head-to-tail assembly, which results in distinct physical and chemical properties. For instance, in comparison with the J-type aggregates, the H-type aggregates possess high crystallinity, fewer stacking defects, and larger π -electron delocalization, thus resulting in a narrower bandgap, higher mobility, and faster carrier separation capacity, beneficial for photocatalytic H₂ production. However, the excessive π - π stacking in H-type structures is predisposed to form oversized supramolecular semiconductors, which greatly diminish their specific surface area and reduce the density of exposed active sites, seriously hampering their practical applications.

Enormous effort has been devoted to developing new methodologies for restricting or regulating the excessive growth of H-type aggregates, in which the hybridization of organic semiconductors with other inorganic functional semiconductors has been proven an efficient protocol. Thereinto, TiO₂ as a classical metal oxide semiconductor has shown great potential in photocatalysis owing to its low-cost, non-toxic, and catalytically active features.^[12] For instance, Zhu group contributed a series of perylene diimide (PDI)-based supramolecular photocatalytic systems, which present broad-spectrum responsiveness and strong redox ability ascribed to the synergistic effects between the self-assembled PDI aggregates and other functional semiconductors,^[13] such as Zn_xCd_yS,^[14] TiO₂,^[15] and C₃N₄.^[16] Impressively, the PDI@TiO₂ composite with a semi-core-shell structure obtained from the integration of PDI precipitate and TiO₂ colloid showcases a full-spectrum response capacity and enhanced photoelectric conversion efficiency,^[15] which provides valuable guidance for modifying the optical properties and photocatalytic activity of the self-assembled supramolecular aggregates by combining them with other inorganic semiconductors.

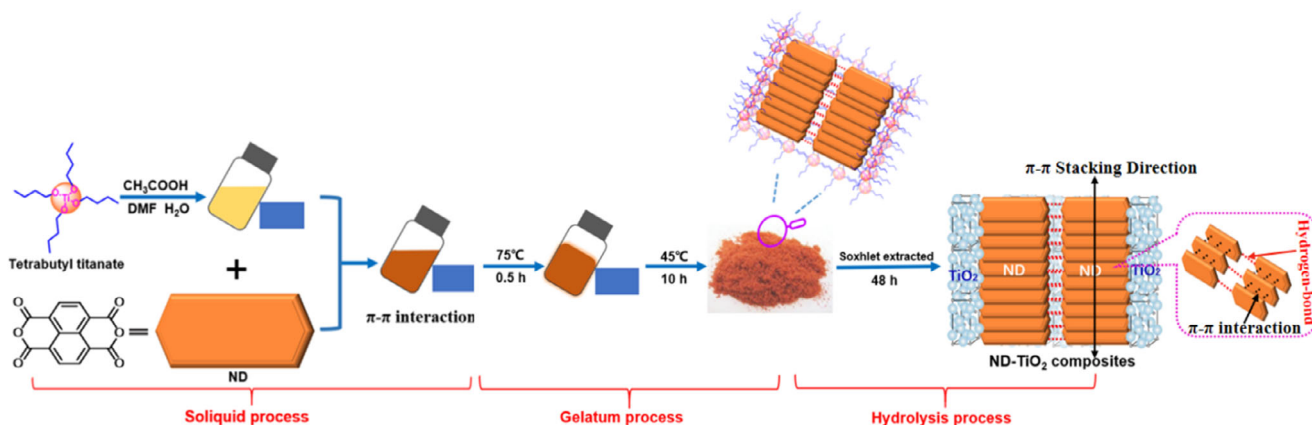
Recently, research has become increasingly focused on the synthesis of H-type PDI-based supramolecular organic semiconductors and their composites for photocatalysis. However, the photocatalytic applications of supramolecular semiconductors based on 1,4,5,8-naphthalenetetracarboxylic dianhydride (ND)

and their diimide derivatives (NDI) are still rare. In fact, ND and NDI can be assembled into supramolecular semiconductors with similar optical activity as PDI-based semiconductors, thus enabling them with good photocatalytic performance. Furthermore, the better solubility of ND/NDI in organic solvents makes their structural modification more straightforward with enhanced flexibility.^[17] For instance, Zhu et al. designed and prepared naphthalimide-substituted porphyrin nanowires and naphthalimide-porphyrin doped graphitic carbon nitride, which show outstanding photocatalytic activity on splitting water for hydrogen production.^[16b,c] These excellent works manifest the promising potential of self-assembled NDI derivatives aggregates through π - π stacking in the field of photocatalytic water splitting. However, the pursuit of new synthesis methodologies for constructing highly efficient, robust, and easily industrialized ND/NDI-based organic photocatalysts is still indispensable.

Herein, we have successfully constructed a series of binary photocatalytic composites, denoted as ND-TiO₂ (*x*:*y*) (*x* and *y* represent the ratios of ND and TiO₂, respectively), from the π - π stacked 1,4,5,8-naphthalenetetracarboxylic dianhydride (ND) and TiO₂ colloid through an in-situ sol-gel method. The combination of the self-assembly process of ND with the hydrolysis-condensation process of tetrabutyl titanate simplifies the preparation process and homogenizes the organic and inorganic components in the composite system. Pt nanoparticles (NPs) (0.5 wt%), serving as a co-catalyst, were introduced into the composite to enhance the photocatalytic activity, of which the actual mass ratio is 0.38 wt% affirmed by ICP-AES (Table S1, Supporting Information). Significantly, the photocatalytic hydrogen evolution rate of ND-TiO₂ (1:10) is ≈ 3.23 mmol·g⁻¹·h⁻¹ under visible-light ($\lambda > 400$ nm) irradiation, corresponding to the TON and TOF values of 2446 and 163.1 h⁻¹, which is enhanced dramatically by 104 and 119 times compared with the parent ND organic semiconductor (0.031 mmol·g⁻¹·h⁻¹) and TiO₂-Colloid (0.027 mmol·g⁻¹·h⁻¹), respectively, as a result of the effective synergistic effects between the ND semiconductor and TiO₂. Additionally, comprehensive experiments have been performed to establish the underlying photocatalytic mechanism, with additional insight garnered from theoretical simulations.

2. Results and Discussion

Scheme 1 represents the synthetic route of ND-TiO₂ composites, including soliquid, gelatum, and hydrolysis processes. First, tetrabutyl titanate was dissolved in acetic acid and then added DMF solution containing ND molecules to obtain a transparent and uniform dark yellow soliquid solution. ND self-assembles into supramolecular nanofibers through π - π stacking interaction between perylene rings and hydrogen bonding side chains as depicted in Scheme 1. Simultaneously, tetrabutyl titanate rapidly forms a 3D cross-linked network gelatum mixture via hydrolysis and condensation reactions. Thus, the electron-rich self-assembled ND and the polyhydroxy titanate gelatum intermediate can be successfully integrated via intermolecular hydrogen bonds or coordination bonds (Ti-O), which may regulate the degree of the π - π stacking for improving the structural and functional compatibility of ND and TiO₂. In contrast, the ND monomers form excessive π - π stacked nanorods of large size (diameter: 1–3 μ m, length: >10 μ m) (**Figure 1a**). The high degree of



Scheme 1. The schematic synthetic route of the ND-TiO₂ composite.

π - π stacking imposes higher electron density and faster charge migration rate. However, the severe photogenerated carrier recombination effect caused by the overgrowth of ND monomers results in unsatisfactory photocatalytic activity. Furthermore, excessive H-type π - π stacking in one direction usually leads to densely packed non-porous structures, which is adverse for the separation and transfer of the photogenerated charge carriers. The TiO₂ colloid is made up of nanoscale flower-like clusters with 20–30 nm irregular spherical nanoparticles (Figure 1b). The morphology of ND-TiO₂ composite is distinct from pure ND self-assembled materials or TiO₂-colloids, pointed ends-nanofibers with 80–100 nm length grow closely to form the rodlike or layered structures, demonstrated by TEM and HR-TEM images (Figure 1c). Note that large-scale interlayer spacing usually plays a crucial role in the stacking mode of self-assembled systems. For example, the H-type π - π stacking configuration for PDI-like molecules exhibits an interlayer spacing of \approx 0.38 nm in self-assembled systems.^[14,18] As shown in Figure 1d,e, for ND-TiO₂, a lattice spacing of 0.38 nm is predominantly observed in the central section of nanofibers for the self-assembled ND, con-

sistent with an H-type π - π stacking configuration. Additionally, a d-spacing of 0.35 nm is observed, which can be assigned to the spherical titanium dioxide particles (Figure 1e). It should be noted that the TiO₂ in ND-TiO₂ encircles the self-assembled ND, forming a type of distinct core-shell structure, in which the π - π stacking states may be influenced through interfacial hydrogen-bond and/or coordination-bond interactions (Figure 1e).

In this system, Pt NPs are loaded on the surface of catalysts and serve as a co-catalyst, which can reduce the overpotential during the photocatalytic H⁺ reduction reaction. Figure 1f,g presents the morphology photographs of the composite ND-TiO₂ (1:10) after photo-depositing Pt NPs on ND-TiO₂ materials, which reveals the distance spacing of 0.21 nm between two adjacent lattice fringes attributed to the (111) plane of Pt NPs and the distribution size of Pt NPs with the value of \approx 5 nm. The EDX analysis results demonstrate the existence of Ti, O, C, and Pt elements in Pt@ND-TiO₂ (1:10), further confirmed by the elemental mapping images, in which the Ti, O, C, and Pt elements are evenly distributed throughout the whole hybrid material (Figure 1h; Figure S1, Supporting Information).

To probe the chemical composition and the coordination state of samples, XPS measurements for TiO₂-Colloid, ND-TiO₂(1:10), and Pt@ND-TiO₂(1:10) were executed and analyzed (Figure S2 and Table S2, Supporting Information). All the samples possess similar elemental compositions of Ti, O, and C, yet with different C ratios (Table S2, Supporting Information). The signal peaks located at 464.5 and 458.6 eV correspond to Ti 2p_{1/2} and Ti 2p_{3/2}, respectively (Figure S2a–c, Supporting Information). For Pt, there are four peaks in the Pt 4f spectral region (Figure S2c, Supporting Information). The signal peaks at 74.6 and 71.3 eV are assigned to Pt 4f_{5/2} and Pt 4f_{7/2}, which are attributed to Pt (0) in agreement with the HRTEM results of Pt (111) (Figure 1g). There are also two peaks at 72.3 and 76.0 eV, indicating the presence of Pt²⁺ in the system, presumably due to the incomplete reduction of K₂PtCl₄ during the photocatalytic process. Compared with the TiO₂-Colloid, the higher C content in ND-TiO₂(1:10) suggests the successful integration between the self-assembled ND and TiO₂-Colloid (Table S2, Supporting Information). After loading Pt NPs, the C content in Pt@ND-TiO₂ decreased compared with ND-TiO₂(1:10), which is ascribed to highly dispersed Pt NPs covering the surface of ND-TiO₂ (1:10) materials

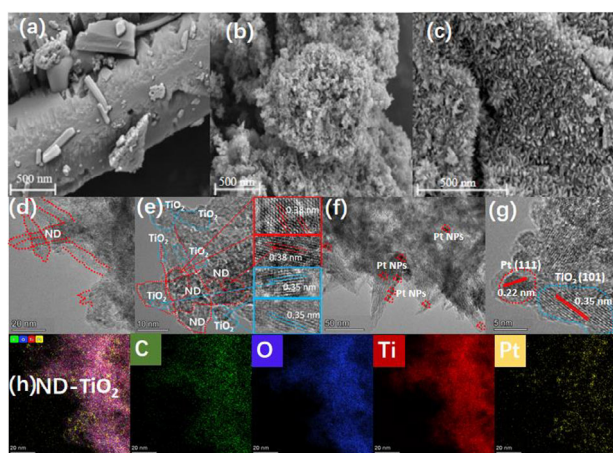


Figure 1. a) SEM images of ND. b) SEM images of TiO₂-Colloid. c–e) SEM, TEM, and HRTEM images of ND-TiO₂ composite. f–h) TEM, HRTEM, and the mapping images of Pt@ND-TiO₂ composite.

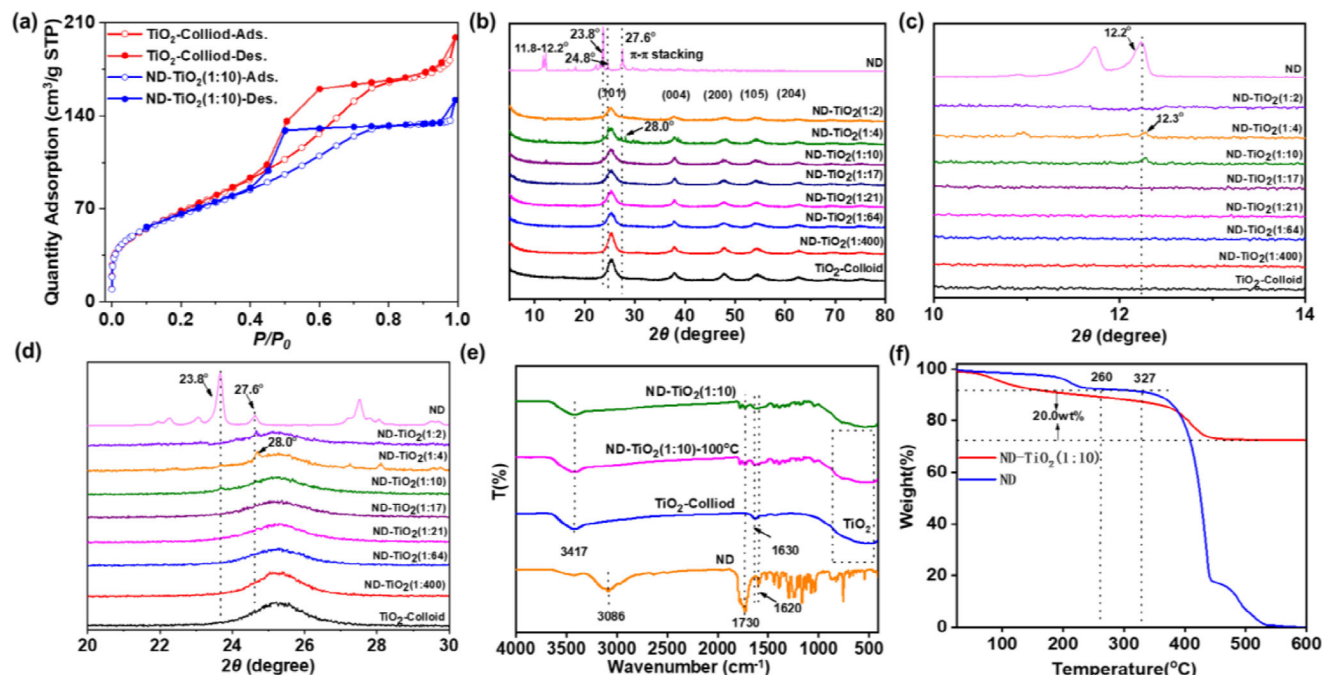


Figure 2. a) The N_2 adsorption isotherms of TiO_2 -Colloid and $ND-TiO_2(1:10)$. b) The XRD patterns of ND, TiO_2 -Colloid, and $ND-TiO_2(x:y)$. c, d) Enlarged PXRD patterns of ND, TiO_2 -Colloid, and $ND-TiO_2(x:y)$. e) FT-IR spectra of ND, TiO_2 -Colloid, and $ND-TiO_2(1:10)$. f) Thermogravimetric curves of TiO_2 -Colloid and $ND-TiO_2(1:10)$.

(Table S2, Supporting Information). As shown in Figure S2a (Supporting Information), for TiO_2 -colloid, there are three signal peaks located at 284.8, 286.2, and 288.8 eV, which are assignable to the C characteristic peaks from the adventitious carbon, C–O and C=O groups from the residual precursors and additives, respectively. In comparison, the C 1s spectra of $ND-TiO_2(1:10)$ and $Pt@ND-TiO_2(1:10)$ show four main characteristic peaks at 291.6, 288.7/288.8, 286.1, and 284.8 eV (Figure S2b,c, Supporting Information), which can be assigned to the $\pi-\pi^*$ satellite, C=O, C–O, and C–C/C–H/C=C groups, respectively. Additionally, the intensity of the peaks at 284.8, 286.1, and 288.8 eV in $ND-TiO_2(1:10)$ is higher than that of TiO_2 -Colloid, further confirming the combination of self-assembled ND with TiO_2 . For the O 1s spectra, TiO_2 -Colloid shows three peaks located at 529.9, 530.8, and 532.0 eV, corresponding to Ti–O, C=O, and C–O, respectively. In comparison, the peaks of C–O and C=O in $ND-TiO_2(1:10)$ and $Pt@ND-TiO_2(1:10)$ shift to 532.1 eV and 531.2 eV (Figure S2b,c, Supporting Information), indicative of the existence of strong intermolecular interactions between ND and TiO_2 . The new binding energy signal peak at 533.5 eV can be attributed to the O 1s spectra arising from the adsorbed H_2O on the surface of $ND-TiO_2(1:10)$ and $Pt@ND-TiO_2(1:10)$, which enhances the hydrophilicity of the composites, confirmed by the water contact angle measurements (Figure S3, Supporting Information). N_2 adsorption isotherms were carried out to evaluate the permanent porosity of TiO_2 -Colloid, ND, and $ND-TiO_2(1:10)$ composites (Figure 2a; Figure S4, Supporting Information). Both TiO_2 -Colloid and $ND-TiO_2(1:10)$ display the mesoporous type IV sorption curves, while ND exhibits the mesoporous type II sorption curve. $ND-TiO_2(1:10)$ presents much higher BET surface area ($237.8\text{ m}^2\text{ g}^{-1}$) than ND ($4.7\text{ m}^2\text{ g}^{-1}$), but slightly lower

than TiO_2 -Colloid ($256.4\text{ m}^2\text{ g}^{-1}$) (Table S3, Supporting Information). The pore size distribution of $ND-TiO_2(1:10)$ based on the BJH (Barrett-Joyner-Halenda) method was estimated to be 3.74 nm, smaller than that of TiO_2 -Colloid (4.17 nm) and ND (16.6 nm) (Figures S4 and S5, Table S3, Supporting Information), which further corroborates the successful hybridization of ND with TiO_2 . Notably, the introduction of TiO_2 into self-assembled ND not only endows the framework with increased surface area, but also enhances the hydrophilicity of the composite, thus providing the possibility of improved photocatalytic H_2 evolution performance.

The PXRD patterns for self-assembled ND, TiO_2 -Colloid and $ND-TiO_2$ composites were performed to examine their phase purity (Figure 2b–d). For TiO_2 -Colloid, the diffraction peaks located at 25.5° , 38.0° , 48.1° , 54.1° , and 62.9° belong to the standard peaks of anatase type TiO_2 , corresponding to the (101), (004), (200), (105), and (204) crystal planes, indicating the formation of TiO_2 with anatase type (JCPDS 21–1272). The characteristic diffraction peaks of ND at 11.8° and 12.2° correspond to the in-plane repeated aromatic rings, and those at 24° – 28° can be attributed to the typical planar $\pi-\pi$ stacking of ND molecules with d-spacings of 0.32–0.38 nm.^[19] Especially, the diffraction peak of 27.6° is ascribed to a d-spacing of 0.32 nm, which is typically the H-type $\pi-\pi$ stacking interaction between ND molecules. For $ND-TiO_2$, the intensity of the peak at 25.5° gradually decreases while the peaks at 12.4° , 23.8° , 24.8° , and 27.6° gradually increase along with the increased ND component in $ND-TiO_2$, suggesting the efficient combination of ND and TiO_2 (Figure 2c,d). Additionally, compared with the parent ND aggregates, the peak located at 27.6° in the pristine ND shifts to 28.0° , unveiling a decreased $\pi-\pi$ stacking spacing in the hybrid material (Figure 2d).

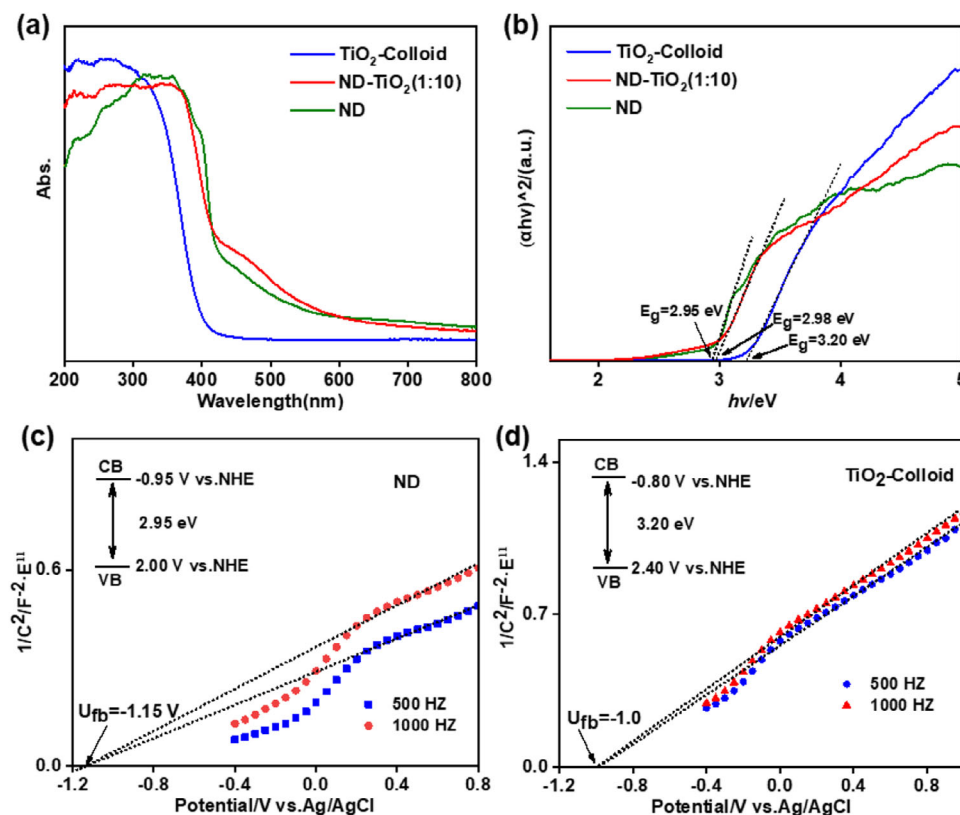


Figure 3. a,b) Solid UV-vis absorption spectra and Tauc plots of TiO₂-Colloid, self-assembled ND, and ND-TiO₂(1:10). c,d) Mott-Schottky diagrams of ND and TiO₂-Colloid.

The FT-IR spectra of ND, TiO₂-Colloid, and ND-TiO₂(1:10) are shown in Figure 2e. ND exhibits two obvious peaks at 3086 and 1730 cm⁻¹, corresponding to the characteristic stretching vibration of the carbonyl group, which confirms the existence of acid anhydride. The characteristic absorption peaks at 3417 and 1630 cm⁻¹ are ascribed to the stretching and bending vibrations of the hydroxyl groups (-OH) on the surface of the TiO₂-Colloid. The composite ND-TiO₂(1:10) exhibits the characteristic vibrational bands of C=C, -OH, C=O, and Ti-O at 1620, 1630, 1730, and 500-700 cm⁻¹, respectively, indicating the successful integration of ND and TiO₂ in the hybrid material. For quantitative analysis of the constituent ratio of ND-TiO₂(1:10) composite, the thermogravimetric plots of self-assembled ND and ND-TiO₂(1:10) were performed under an air atmosphere from 25 to 600 °C (Figure 2f). These results reveal that the self-assembled ND is stable up to 327 °C, whereas the ND-TiO₂(1:10) tends to decompose after 400 °C. The weight loss region of 20% from 260 to 600 °C in the TGA curves represents the ND mass ratio in ND-TiO₂(1:10) composite, in good agreement with the theoretical value ($\approx 25.1\%$).

The solid-state UV-vis absorption spectra of TiO₂-Colloid, self-assembled ND, and ND-TiO₂(1:10) were conducted to evaluate their optical responsiveness performance. As depicted in Figure 3a, the ND exhibits broadly intense optical absorbance below 600 nm and extends to over 800 nm. TiO₂-Colloid shows a narrow absorbance below 400 nm. After introducing ND into TiO₂, the composite ND-TiO₂(1:10) displays significantly enhanced absorbance with the self-assembled ND in the visible

light and the near infrared light region. The band gaps of TiO₂-Colloid, self-assembled ND, and ND-TiO₂(1:10) are calculated to be 3.20, 2.95, and 2.98 eV, respectively (Figure 3b), suggesting that the merger of self-assembled ND with TiO₂ effectively tunes the band gap width. It should be noted that the π - π stacking interactions and modes of ND molecules not only can effectively narrow the band gaps of ND compared with the isolated ND molecule (3.69 eV calculated by DFT methods at the B3LYP/6-31G(d) level), but also can confer the ND-TiO₂(1:10) composite with different delocalized charge transfer capacity along the π - π stacking direction, affecting the accumulation and utilization efficiency of the photogenerated charges, therefore DFT calculations were implemented to investigate the effect of stacking arrangements on the energy level structures (Figure S6 and Table S4, Supporting Information). The analysis of the entire energy change shows that the π - π stacking states between two individual ND molecules (1) tend to be arranged in the way of (2), wherein the coplanar molecules stack directly along the z-axis in an AA manner with 3.4 Å planar separation and complete overlap of molecular orbitals. Deviation from the 3.4 Å separation was probed in the series of (3), (4), and (5), with 2.3, 2.9, and 4.0 Å spacing, respectively. Deviation from the optimal 3.4 Å spacing was found to decrease or increase the bandgap proportional to the change in distance, while the experimental bandgap (2.95 eV) was most similar to the optimized 3.4 Å of (2) (Figure 3b; Figure S6, Supporting Information). Deviation from planarity was explored in arrangements (6) and (7) with 30° and 60° angles imposed

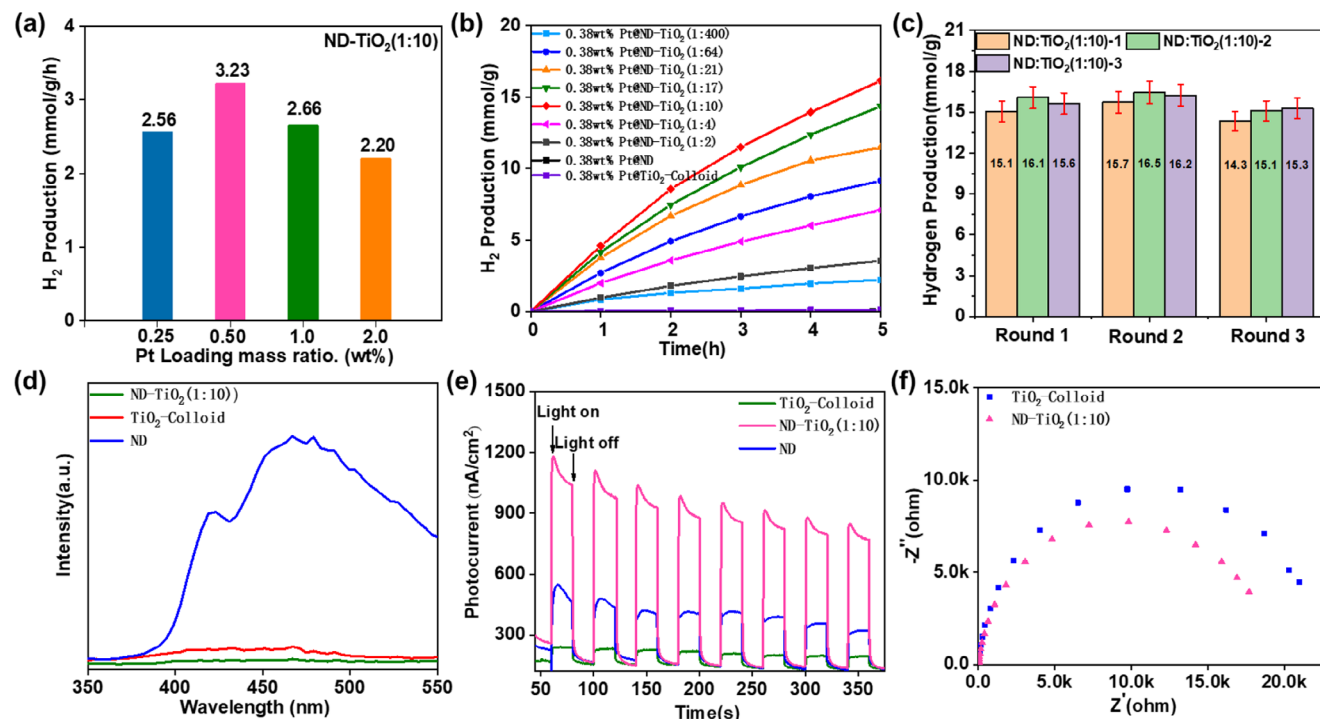


Figure 4. a) The photocatalytic hydrogen production performance over ND-TiO₂(1:10) with different Pt loading mass amounts. b) The photocatalytic hydrogen production performance over 0.38 wt% Pt@ND-TiO₂ with different ND doping mass, 0.38 wt% Pt@ND, and 0.38 wt% Pt@TiO₂-Colloid. c) The photocatalytic cycle experiments under visible light irradiation ($\lambda > 400$ nm) over different batches of 0.38 wt% Pt@ND-TiO₂(1:10)-1/2/3 samples at 20 mL H₂O/TEOA (9:1, v/v). d) The steady-state solid photoluminescence spectra of self-assembled ND, TiO₂-Colloid, and ND-TiO₂(1:10). e) Transient photocurrent response plots of TiO₂-Colloid, self-assembled ND, and ND-TiO₂(1:10). f) The electrochemical impedance plots of TiO₂-Colloid and ND-TiO₂(1:10).

between the molecular planes, respectively. The angular deviation from coplanarity resulted in significant ground-state energy increases of 718.93 kJ mol⁻¹ and 732.08 kJ mol⁻¹ for arrangements (6) and (7) respectively (Table S4, Supporting Information) relative to the optimal coplanar (2), and the bandgap increased by 0.33 eV over (2) for both cases. The addition of a 3rd coplanar ND molecule and analysis of the bandgap were examined in AAA, ABA, and ABC stacking arrangements (8), (9), and (10), respectively. Notably, the ABA (9) and ABC (10) arrangements are comparable in ground-state energy at ~ 50 kJ/mol below the AAA (8) stacking arrangement, but both (9) and (10) were found to increase the bandgap by 0.47 eV relative to (8). Finally, in-plane arrangement of ND molecules (11) results in a negligible bandgap deviation (-0.06 eV) relative to the isolated monomer (1). Note that the migration of photogenerated electrons is usually limited to a short distance along the π - π stacking direction due to the resistance of electron transfer. The integration of TiO₂ with self-assembled ND through the external interactions like hydrogen bonds (-OH on the surface of TiO₂) or coordination bonds (Ti-O) may break the π - π stacking equilibrium and limit the overgrowth of ND to some extent, thereby adjusting the optical properties and photocatalysis performance of self-assembled ND. These results suggest that the ND molecules in ND-TiO₂(1:10) are arranged in the way of (2). To determine the flat-band potentials and determine the electron transfer process during the photocatalytic reaction, Mott-Schottky (M-S) measurements of TiO₂-Colloid and self-assembled ND were carried out at differ-

ent frequencies (500 and 1000 Hz) (Figure 3c,d). The positive slopes of the Mott-Schottky curves signify an n-type semiconductor. Considering that the conduction band nearly equates to the flat-band potential (U_{fb}) in n-type semiconductors,^[18] the conduction band (CB) potentials of self-assembled ND and TiO₂-Colloid are ≈ -0.95 and -0.80 eV, respectively (vs NHE), demonstrating adequate ability for photocatalytic proton reduction. The valence band (VB) positions of self-assembled ND and TiO₂-Colloid are estimated to be 2.0 and 2.4 eV, respectively. Notably, the CB and VB positions of self-assembled ND are higher than those of TiO₂-Colloid, which allows the formation of an II-type interlaced heterojunction structure between the self-assembled ND and TiO₂-Colloid, thus facilitating the separation and followed migration of photogenerated charge carriers.

Prompted by the excellent optical responsiveness, matching band gap, and hierarchical pore structure, the photocatalytic H₂ evolution experiments on Pt@ND-TiO₂ were performed under visible-light irradiation ($\lambda > 400$ nm). Given that the Pt NPs play a pivotal role in the reaction system, the loading amounts of Pt NPs (0.25/0.50/1.0/2.0 wt%) were first systematically optimized, manifesting the optimum Pt NPs loading amount of 0.38% (Figure 4a; Table S1, Supporting Information). As the introduced amounts of ND into TiO₂ also influence the photocatalytic activity of the resultant ND-TiO₂ composites, a series of hetero-structure composites with different amounts of ND were synthesized through the in situ sol-gel protocol, and followed by 0.38 wt% Pt NPs being loaded on their surface. Through

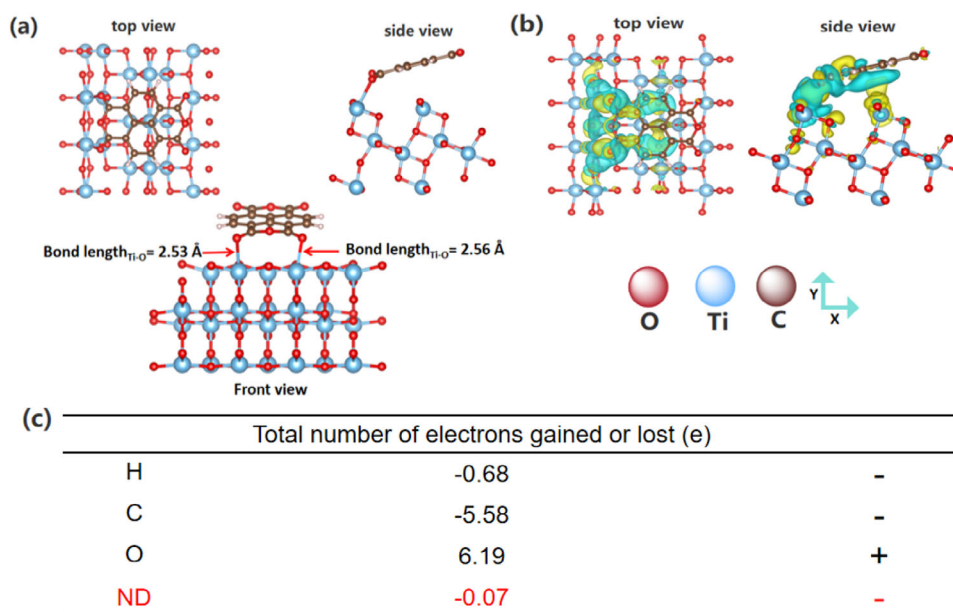


Figure 5. a) The optimized structure on the adsorption configuration of ND molecules onto TiO_2 : Top view, Side view, and Front view. b) The 3D differential charge density of ND molecules adsorbed onto TiO_2 . c) The Bader analysis of ND.

the optimization experiments, the best photocatalytic composite, 0.38 wt% $\text{Pt@ND-TiO}_2(1:10)$ is identified, showing the maximum photocatalytic H_2 evolution rate of $3.23 \text{ mmol}\cdot\text{g}^{-1}\cdot\text{h}^{-1}$, comparable with many reported ND/PD-based photocatalysts (Table S5, Supporting Information). It is worth noting that the H_2 evolution rate on $\text{Pt@ND-TiO}_2(1:10)$ is much higher than its parent counterparts, $\text{Pt@TiO}_2\text{-Colloid}$ ($0.027 \text{ mmol}\cdot\text{g}^{-1}\cdot\text{h}^{-1}$) and Pt@ND ($0.031 \text{ mmol}\cdot\text{g}^{-1}\cdot\text{h}^{-1}$), demonstrating the effectiveness of synergy through the combination of $\pi\text{-}\pi$ stacking ND aggregate with $\text{TiO}_2\text{-Colloid}$ (Figure 4b). Additionally, to examine the repeatability of the photocatalyst, three batches of $\text{ND-TiO}_2(1:10)$, named $\text{ND-TiO}_2(1:10)\text{-1/2/3}$, were synthesized and used to perform the photocatalytic H_2 evolution, which reveals good reproducibility of the $\text{ND-TiO}_2(1:10)$ composite (Figure S7a, Supporting Information). Considering that the gradually decreasing H_2 evolution rate is a prevalent issue in photocatalytic reaction process, probably due to the deactivation of catalytic active sites or the instability of the catalyst under prolonged light irradiation, the cyclic experiments were executed as depicted in Figure 4c, the $\text{Pt@ND-TiO}_2(1:10)$ composite maintains its high activity even after 3 rounds of experiments (15 h), confirming its good photocatalytic durability and recyclability. The cycle experiments based on three different batches of $\text{ND-TiO}_2(1:10)\text{-1/2/3}$ samples were also performed under the optimized reaction condition, further confirming its good photocatalytic stability and reproductivity (Figure 4c; Figure S7b, Supporting Information). PXRD, SEM, TEM, and XPS spectra reveal that $\text{Pt@ND-TiO}_2(1:10)$ composite still retains structure integrity and high crystallinity after the recycling experiment (Figure S8, Supporting Information). The TON value based on the mole numbers of Pt NPs loaded on the surface of ND-TiO_2 composite is estimated to be 2446, corresponding to the TOF value of 163.1 h^{-1} .

To probe the electron transfer process from self-assembled ND to TiO_2 , steady-state solid photoluminescence was con-

ducted, revealing the following fluorescence intensity order of self-assembled ND > $\text{TiO}_2\text{-Colloid}$ > $\text{ND-TiO}_2(1:10)$, indicating the significantly enhanced excitation dissociation and charge separation/transportation, both beneficial to the photocatalytic H_2 evolution (Figure 4d). The separation and transport performance of charge carriers is a vital metric for the photocatalytic H_2 evolution. Therefore, a series of photoelectrochemical experiments involving the photocurrent responses and the electrochemical impedance spectroscopy (EIS) were implemented to assess the kinetics of charge separation and migration (Figure 4e,f). As presented in Figure 4e, compared with the parent $\text{TiO}_2\text{-Colloid}$ and ND aggregate, $\text{ND-TiO}_2(1:10)$ composite exhibits the highest photocurrent response intensity, indicating that the charge carrier separation and transport on TiO_2 have been significantly enhanced after introducing the appropriate amounts of self-assembled ND. In addition, the Nyquist plots of EIS further validate the results, in which the $\text{ND-TiO}_2(1:10)$ composite shows a smaller arc radius than the parent $\text{TiO}_2\text{-Colloid}$ (Figure 4f).

To further demonstrate the charge transfer mechanism between ND and TiO_2 , the differential charge and Bader of ND molecules adsorbed onto TiO_2 were evaluated. The optimized structure of the adsorption configuration of ND molecules onto the surface of TiO_2 is shown in Figure 5a. The differential charge density plot of the adsorption configuration of ND molecules with the isosurface of $0.0005 \text{ e}\cdot\text{\AA}^{-3}$, involving top view and side view, is shown in Figure 5b, in which the blue part wrapped represents electron dissipation, and the yellow part represents electron aggregation. It can be observed that there is a strong redistribution of charge. In the ND molecule, the oxygen atom is covered by the yellow area, which is manifested as electron aggregation. Both of the C and H atoms are covered by the blue area, which displays an electron consumption area. The overall charge distribution map between the entire ND molecule and TiO_2 indicates that a strong electron transfer exists between the ND molecule

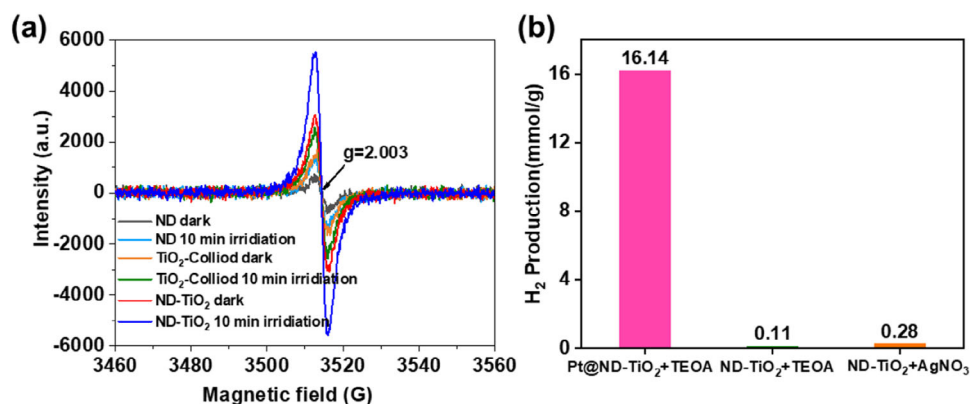


Figure 6. a) The EPR spectra of TiO₂-Colloid, self-assembled ND, and ND-TiO₂ in the dark and under visible light irradiation. b) The photocatalytic H₂ evolution of ND-TiO₂(1:10) materials with Pt loading, ND-TiO₂(1:10) materials without Pt loading, and ND-TiO₂(1:10) with AgNO₃ as electron scavenger.

and TiO₂. In Figure 5c, the Bader charge calculation shows that the sum of electrons gained or lost in the whole ND molecule appears as a negative value, indicating that the whole ND molecule loses electrons. And the electrons could transfer from the ND molecule to TiO₂ with an overall transferred electron number of 0.07e, which is consistent with the above differential charge map situation, thus manifesting the charge transfer pathway between ND and TiO₂.

To assess the ability to produce photogenerated electrons, electron paramagnetic resonance (EPR) measurements were performed. As shown in Figure 6a, a single peak at $g = 2.003$ assigned to the photoexcited electron is detected in the magnetic fields between 3510 and 3520 G for TiO₂-Colloid, self-assembled ND, and ND-TiO₂(1:10), indicating the feasibility of generating electrons during the photocatalytic reaction. Notably, the EPR intensity significantly increases after illuminating the samples of TiO₂-Colloid, self-assembled ND, and ND-TiO₂(1:10) for several minutes, manifesting the vital role of light. Compared with TiO₂-Colloid and self-assembled ND, ND-TiO₂(1:10) displays the most intense EPR signal, signifying that most photogenerated electrons on ND-TiO₂(1:10) can be afforded upon visible-light irradiation consistent with the effective truncation of ND π - π stacking afforded by the introduction of TiO₂ into the self-assembled ND and the establishment of electronic coupling at the interface between the organic and inorganic components.^[14c]

It is important to note that factors that influence photocatalytic performance are various, apart from the photogenerated charge separation and transfer on the interface, which might be affected by overpotential or the oxidation of the sacrificial donor by the holes. The former can be resolved by the introduction of co-catalysts (Pt, Pd, Ni, etc.), which can efficiently decrease the overpotential during the photocatalytic process. As shown in Figure 6b, the photocatalytic H₂ evolution rate on ND-TiO₂(1:10) composite with Pt NPs is 3.23 mmol·g⁻¹·h⁻¹, which is 166 times higher than that of ND-TiO₂(1:10) composite (0.020 mmol·g⁻¹·h⁻¹) without Pt NPs, indicative of the crucial role of Pt NPs in the photocatalytic reaction process. For the latter, as the sacrificial donor can eliminate the holes to avert photogenerated charge recombination, the commonly used triethanolamine (TEOA) as an organic sacrificial donor is chosen in this sys-

tem. However, the oxidation of the organic sacrificial donor, $C_6H_{15}NO_3 + 12H_2O + nH^+ \rightarrow 6CO_2 + 19H_2 + HNO_3$, has been proposed to directly produce H₂ in aqueous photo-catalysis or a photocatalytic system of water splitting.^[20] Therefore, it is necessary to evaluate the contribution of the photocatalytic reduction of H⁺ efficiency from the oxidation of the organic sacrificial agent. The H₂ production rate of ND-TiO₂(1:10) with AgNO₃ as electron eliminator, which can exclude the interference of the proton reduction by electrons, is ≈ 0.060 mmol·g⁻¹·h⁻¹, which is 3 times higher than that of ND-TiO₂(1:10) without AgNO₃ (Figure 6b), but much less than that of ND-TiO₂(1:10) composite with Pt NPs as co-catalyst and TEOA as sacrificial agent. The results show that the oxidation of the organic sacrificial donor indeed occurs in this system, but the contribution to the total H₂ production is negligible. Overall, it can be concluded that the self-assembled ND, TiO₂, and Pt NPs synergistically contribute to the enhanced H₂ evolution performance via rational integration of ND with TiO₂ and followed by Pt NPs deposition.

In view of the above experimental and theoretical results, the photocatalytic mechanism is proposed in Figure 7. For Pt@ND-TiO₂(1:10), the self-assembled ND serves as the antenna to absorb visible light, in which the photogenerated electrons jump

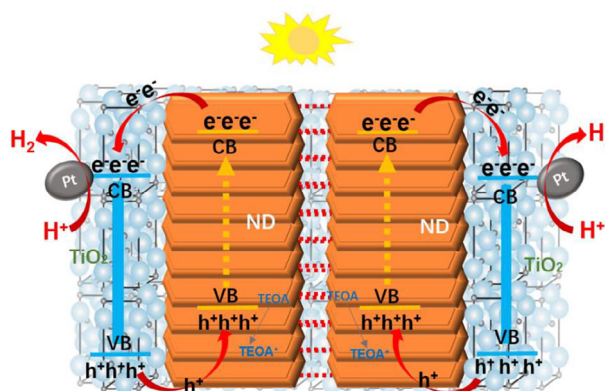


Figure 7. The photocatalytic H₂ evolution mechanism over ND-TiO₂ composite.

onto the CB while the holes are retained on the VB. Then the photogenerated electrons in the CB of self-assembled ND transfer to the CB of TiO₂ which can be ascribed to the more negative CB of self-assembled ND, whereas the holes in the VB of TiO₂, in turn, transfer to the VB of self-assembled ND smoothly due to the higher VB energy of TiO₂, thus guaranteeing the fast charger carriers' separation and immigration. Subsequently, accumulated photoexcited electrons on the CB of TiO₂ transfer to the Pt NPs surface for the H⁺ reduction, while the holes on the VB of self-assembled ND are captured by the sacrificial agent, TEOA, closing the photocatalytic cycle.

3. Conclusion

In summary, we have developed a series of photosensitive porous composites, ND-TiO₂(x:y), featuring excellent optical response, fast separation and migration ability of photo-induced charge carriers, as well as permanent porosity, through the self-assembled integration of the π - π stacking ND with TiO₂-colloid via an in-situ sol-gel strategy, for photocatalytic H₂ production. Notably, the combination of TiO₂ with ND effectively restrains the overgrowth of ND self-assembly, resulting in the formation of a porous structure that shortens the charge transfer distance, whereas the introduction of ND into the TiO₂-colloid, in turn, enhances the visible-light response and promotes charge carrier separation and migration attributable to the excellent visible-light absorbance of ND self-assembly and the matching band gap between ND and TiO₂, thus giving rise to the significantly improved photocatalytic H₂ evolution performance. The optimized Pt@ND-TiO₂(1:10) presents a maximum H₂ evolution rate of 3.23 mmol·g⁻¹·h⁻¹, with extraordinary TON (2446) and TOF (163.1 h⁻¹) values, greatly exceeding the constituent ND (0.031 mmol·g⁻¹·h⁻¹) and TiO₂-Colloid (0.027 mmol·g⁻¹·h⁻¹) counterparts. Finally, comprehensive experiments and theoretical simulations have been designed and performed to unveil the underlying photocatalytic mechanism, in which the excellent visible-light responsiveness, well-matched band gap, as well as porous structural feature, jointly lead to superior photocatalytic performance, and can be ascribed to the synergistic effects of ND self-assembly and TiO₂ stemming from their rational assembly. This work may serve as inspiration for the rational design and synthesis of more novel organic/inorganic hybrid materials for practical applications in the field of photocatalysis.

4. Experimental Section

Chemicals and Materials: 1,4,5,8-Naphthalenetetracarboxylic anhydride (ND), acetic acid, tetrabutyl titanate, methanol (MeOH), potassium tetrachloroplatinate (II), super-dry N, N-dimethylformamide (DMF), and triethanolamine (TEOA) were purchased from Shanghai Aladdin Biochemical Technology Co. All reagents were used directly without additional purification.

Catalyst Preparation—Synthesis of ND-TiO₂ Materials: The combination of self-assembly and in situ sol-gel process was used to prepare series of ND-TiO₂ composites. After successively adding 20 mL of anhydrous DMF, 1.5 mL of acetic acid, and 1 mL of deionized water into a glass sample bottle, 10 mL of tetrabutyl titanate was added to the mixed solution. Then, ND (0.744 g) was dissolved in 40 mL of DMF and slowly added to the mixed solution with magnetic stirring and heated at 75 °C until the mixture

become the yellow dry gel state from the solution state. Finally, the yellow gel was washed by the Soxhlet extraction for 48 h and dried in a vacuum oven at 45 °C to obtain the yellow solid, denoted as ND-TiO₂(1:10) composite. Other ND-TiO₂ materials with various mole ratios of ND and TiO₂, denoted as ND-TiO₂(x:y) (x and y represent the ratios of ND and TiO₂, respectively), were prepared, including ND-TiO₂(1:2), ND-TiO₂(1:4), ND-TiO₂(1:17), ND-TiO₂(1:21), ND-TiO₂(1:64), ND-TiO₂(1:400) and TiO₂-Colloid without doping ND, as the above process.

Catalyst Preparation—Synthesis of Pt@ND-TiO₂ Materials: Pt nanoparticles (NPs) (0.16/0.38/0.86/1.5 wt%) were loaded onto the ND-TiO₂(1:10) composite by a photo-deposition method. In general, 30 mg of ND-TiO₂(1:10) composite was dispersed in 20 mL H₂O and MeOH (4:1, v/v) solution with continuous stirring, and K₂PtCl₄ (10 mM, 76.9 μ L) was added slowly dropwise. The mixture was evacuated and replenished with argon 3 times followed by illumination with a 300 W Xe lamp for 30 min. The resulting solid powder was centrifuged, sequentially washed with deionized water and methanol, and dried in a vacuum oven at 45 °C. The actual reduced Pt mass loading on the composite was determined by inductively coupled plasma atomic emission spectrometry (ICP-AES). The theoretical amounts of K₂PtCl₄ added in the synthesis and the corresponding loading amounts of Pt NPs determined are listed in Table S1 (Supporting Information).

Photocatalytic Hydrogen Production: 20 mg samples were dispersed in 20 mL H₂O and TEOA (18: 2, v/v) solution, which was placed in a glass cell with a quartz cover connected to a closed circulation. The reaction system was stirred continuously and cooled at 5 °C by the circulation of cooling water. Then the closed glass cell was evacuated to remove oxygen from the system. Finally, the suspension was illuminated by a 300 W Xe lamp organized with an optical filter ($\lambda > 400$ nm) to cut off the ultraviolet light region. Quantification of hydrogen production was conducted using a Perfect Light system, Beijing Co., Ltd., and the production was detected at an interval of 1 h by an online gas chromatograph (Fu Li GC9790) with a TCD detector. The photocatalytic stability test was implemented for 3 cycles under the same conditions as above. After every photocatalytic hydrogen production test, the catalyst samples are centrifuged and washed with water and methanol, followed by drying.

Supporting Information

Supporting Information is available from the Wiley Online Library or from the author.

Acknowledgements

This research was supported by the Collaborative Innovation Center of Ecological Civilization, Hainan University (XTCX2022STC15), the Project of Sanya Yazhou Bay Science and Technology City (SCKJ-JYRC-2023-13), the National Natural Science Foundation of China (22471294, 22001271, 22002139), Hainan Provincial Natural Science Foundation of China (221QN0858), the National Key Research and Development Program of China (2021YFA0909604), Hainan Province Science and Technology Special Fund (ZDYF2024XDNY268) and the Hainan University Startup Fund (KYQD(ZR)-22104). Partial support from the Robert A. Welch Foundation (B-0027) (S.M.) and Princess Nourah bint Abdulrahman University Researchers Supporting Project (PNURSP2025R1), Riyadh, Saudi Arabia (T.A.) is also acknowledged.

Conflict of Interest

The authors declare no conflict of interest.

Author Contributions

Y.C. and D.K. contributed equally to this work. C.-X.C., S.C., and S.M. performed conceptualization; Y.C., Y.S., P.L., and D.K. performed methodology and investigation; Y.C., H.L., J.C., C.M., and D.K. performed measurements; L.C. and C.-X.C. performed writing-original draft; Y.C., C.-X.C., P.V.,

and S.M. performed writing and review & editing; L.C., Y.C., C.-X.C., Y.S., S.C., P.L., T.A., and S.M. performed funding acquisition. All authors analyzed and discussed the data and contributed to writing the paper.

Data Availability Statement

The data that support the findings of this study are available from the corresponding author upon reasonable request.

Keywords

heterogeneous photocatalyst, naphthalenetetracarboxylic dianhydride, photocatalytic hydrogen evolution, self-assembly, TiO₂

Received: February 15, 2025

Revised: May 5, 2025

Published online:

- [1] a) M. Tayyab, Y. Liu, Z. Liu, Z. Xu, W. Yue, L. Zhou, J. Lei, J. Zhang, *Chem. Eng. J.* **2023**, *455*, 140601; b) R. Zhai, L. Zhang, M. Gu, X. Zhao, B. Zhang, Y. Cheng, J. Zhang, *Small* **2023**, *19*, 2207840; c) X. Zhang, J.-R. Li, *Green. Energy Environ.* **2023**, *8*, 351; d) H. Tong, S. Ouyang, Y. Bi, N. Umezawa, M. Oshikiri, J. Ye, *Adv. Mater.* **2012**, *24*, 229.
- [2] a) Q. Chen, G. Gao, H. Guo, S.-A. Wang, Q. Wang, Y. Fang, X. Hu, R. Duan, *Chem. Eng. J.* **2023**, *470*, 144199; b) Z. Lian, M. Sakamoto, Y. Kobayashi, N. Tamai, J. Ma, T. Sakurai, S. Seki, T. Nakagawa, M. W. Lai, M. Haruta, H. Kurata, T. Teranishi, *ACS Nano* **2019**, *13*, 8356; c) V. W. Lau, I. Moudrakovski, T. Botari, S. Weinberger, M. B. Mesch, V. Duppel, J. Senker, V. Blum, B. V. Lotsch, *Nat. Commun.* **2016**, *7*, 12165; d) B. Lin, Y. Zhou, B. Xu, C. Zhu, W. Tang, Y. Niu, J. Di, P. Song, J. Zhou, X. Luo, L. Kang, R. Duan, Q. Fu, H. Liu, R. Jin, C. Xue, Q. Chen, G. Yang, K. Varga, Q. Xu, Y. Li, Z. Liu, F. Liu, *Mater. Horiz.* **2021**, *8*, 612.
- [3] a) H. Zheng, J. Z. Ou, M. S. Strano, R. B. Kaner, A. Mitchell, K. Kalantar-zadeh, *Adv. Funct. Mater.* **2011**, *21*, 2175; b) Z. Zhang, Q. Wu, G. Johnson, Y. Ye, X. Li, N. Li, M. Cui, J. D. Lee, C. Liu, S. Zhao, S. Li, A. Orlov, C. B. Murray, X. Zhang, T. B. Gunnoe, D. Su, S. Zhang, *J. Am. Chem. Soc.* **2019**, *141*, 16548; c) L. Zhou, J. Meng, P. Li, Z. Tao, L. Mai, J. Chen, *Mater. Horiz.* **2017**, *4*, 268; d) J. Yang, H. Wang, L. Jiang, H. Yu, Y. Zhao, H. Chen, X. Yuan, J. Liang, H. Li, Z. Wu, *Chem. Eng. J.* **2022**, *427*, 130991; e) C. Zhao, Z. Chen, R. Shi, X. Yang, T. Zhang, *Adv. Mater.* **2020**, *32*, 1907296; f) H. Ou, L. Lin, Y. Zheng, P. Yang, Y. Fang, X. Wang, *Adv. Mater.* **2017**, *29*, 1700008; g) C.-X. Chen, Y. Y. Xiong, X. Zhong, P. C. Lan, Z. W. Wei, H. Pan, P. Y. Su, Y. Song, Y. F. Chen, A. Nafady, S. M. Sirajuddin, *Angew. Chem., Int. Ed.* **2022**, *61*, 202114071; h) X. Han, Y. Dong, J. Zhao, S. Ming, Y. Xie, *Int. J. Hydrogen Energy* **2022**, *47*, 18334.
- [4] a) H. Yan, Z. Chen, Y. Zheng, C. Newman, J. R. Quinn, F. Dötz, M. Kastler, *Nature* **2009**, *457*, 679; b) H. Yu, P. Joo, D. Lee, B.-S. Kim, J. H. Oh, *Adv. Opt. Mater.* **2015**, *3*, 241.
- [5] R. S. Loewe, R. K. Lammi, J. R. Diers, C. Kirmaier, D. F. Bocian, D. Holten, J. S. Lindsey, *J. Mater. Chem.* **2002**, *12*, 1530.
- [6] K. Qian, J. Fang, R. Liu, J. Jiang, J. Tong, X. Guo, J. Feng, *Mater. Today Commun.* **2018**, *14*, 254.
- [7] L. Tao, J. Zhao, J. Chen, C. Ou, W. Lv, S. Zhong, *Nanoscale Adv.* **2021**, *3*, 3199.
- [8] L. R. Melby, R. J. Harder, W. R. Hertler, W. Mahler, R. E. Benson, W. E. Mochel, *J. Am. Chem. Soc.* **1962**, *84*, 3374.
- [9] R. Oshi, S. Abdalla, M. Springborg, *Eur. Phys.* **2019**, *73*, 124.
- [10] Y. Sun, Y. Liu, D. Zhu, *J. Mater. Chem.* **2005**, *15*, 53.
- [11] a) D. F. Perepichka, M. R. Bryce, C. Pearson, M. C. Petty, E. J. McInnes, J. P. Zhao, *Angew. Chem. Int. Ed.* **2003**, *42*, 4636; b) X. Lian, Z. Ma, Z. Zhang, J. Yang, Y. Liu, C. Gu, R. Guo, Y. Wang, X. Ye, S. Sun, Y. Zheng, H. Ding, J. Hu, X. Cao, H. Mao, J. Zhu, S. Li, W. Chen, *Surf. Sci.* **2020**, *524*, 146396; c) H. Lin, J. Wang, J. Zhao, Y. Zhuang, B. Liu, Y. Zhu, H. Jia, K. Wu, J. Shen, X. Fu, X. Zhang, J. Long, *Angew. Chem. Int. Ed.* **2022**, *61*, 202117645.
- [12] a) K. Peng, L. Zhang, Y. Xie, Y. Ma, J. Ye, Y. Dai, Y. Chen, L. Wang, W. Zhang, *Fuel* **2024**, *374*, 132460; b) Y. Liu, C. Xu, Y. Xie, L. Yang, Y. Ling, L. Chen, *J. Alloy Compd.* **2020**, *820*, 153440; c) K. Peng, Z. Fan, Y. Wang, Y. Xie, Y. Ling, *Int. J. Hydrogen Energy* **2024**, *60*, 835; d) R. Hou, M. Xu, Z. Fan, R. Zhong, Y. Ling, Y. Wang, *Mater. Today Phys.* **2024**, *44*, 101426; e) X. Mu, M. Xu, Y. Wang, Y. Luo, Y. Xie, Y. Ling, *Int. J. Hydrogen Energy* **2024**, *63*, 1174.
- [13] T. Sun, J. Song, J. Jia, X. Li, X. Sun, *Nano Energy* **2016**, *26*, 83.
- [14] Y. Wei, M. Ma, W. Li, J. Yang, H. Miao, Z. Zhang, Y. Zhu, *Appl. Catal. B: Environ.* **2018**, *238*, 302.
- [15] a) Y. Chen, A. Li, X. Yue, L. N. Wang, Z. H. Huang, F. Kang, A. A. Volinsky, *Nanoscale* **2016**, *8*, 13228; b) D. Liu, J. Wang, X. Bai, R. Zong, Y. Zhu, *Adv. Mater.* **2016**, *28*, 7284; c) W. Wei, Y. Zhu, *Small* **2019**, *15*, 1903933.
- [16] a) S. Chen, C. Wang, B. R. Bunes, Y. Li, C. Wang, L. Zang, *Appl. Catal. A: Gen.* **2015**, *498*, 63; b) Q. Gao, J. Xu, Z. Wang, Y. Zhu, *Appl. Catal. B: Environ.* **2020**, *271*, 118933.
- [17] a) B. Bhavani, N. Chanda, V. Kotha, G. Reddy, P. Basak, U. Pal, L. Giribabu, S. Prasanthkumar, *Nanoscale* **2022**, *14*, 140; b) G. B. Bodedla, J. Huang, W.-Y. Wong, X. Zhu, *ACS Appl. Nano Mater.* **2020**, *3*, 7040; c) L. Li, G. B. Bodedla, Z. Liu, X. Zhu, *Appl. Surf. Sci.* **2020**, *499*, 143755; d) A. Monti, J. M. de Ruiter, H. J. M. de Groot, F. Buda, *J. Phys. Chem. C* **2016**, *120*, 23074.
- [18] N. Meher, P. K. Iyer, *Angew. Chem. Int. Ed.* **2018**, *130*, 8624.
- [19] Y.-F. Chen, L.-L. Tan, J.-M. Liu, S. Qin, Z.-Q. Xie, J.-F. Huang, Y.-W. Xu, L.-M. Xiao, C.-Y. Su, *ACS Energy Lett.* **2017**, *206*, 426.
- [20] F. Costantino, P. V. Kamat, *ACS Energy Lett.* **2022**, *7*, 242.